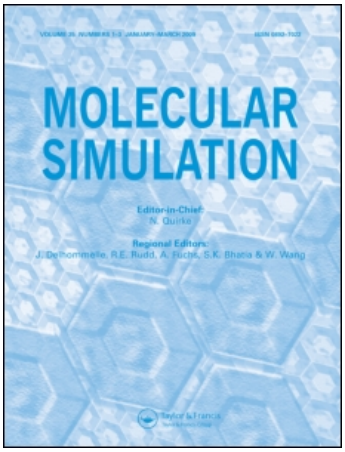

Molecular Simulation
Publication details, including instructions for authors and subscription information:
http://www.informaworld.com/smpp/title~content=t713644482

Integrated atomistic modelling of interstitial defect growth in silicon

Sangheon Lee [a]; Robert J. Bondi [a]; Gyeong S. Hwang [a]
[a] Department of Chemical Engineering, University of Texas, Austin, TX, USA

To cite this Article Lee, Sangheon, Bondi, Robert J. and Hwang, Gyeong S.(2009) 'Integrated atomistic modelling of interstitial defect growth in silicon', Molecular Simulation, 35: 10, 867 — 879
To link to this Article: DOI: 10.1080/08927020902929802
URL: http://dx.doi.org/10.1080/08927020902929802

Molecular Simulation
Vol. 35, Nos. 10–11, September 2009, 867–879

Taylor & Francis
Taylor & Francis Group

Integrated atomistic modelling of interstitial defect growth in silicon

Sangheon Lee, Robert J. Bondi and Gyeong S. Hwang*

Department of Chemical Engineering, University of Texas, Austin, TX 78712, USA

(*Received 22 December 2008; final version received 24 March 2009*)

A new theoretical approach that combines Metropolis Monte Carlo, tight-binding molecular dynamics, and density functional theory calculations is introduced as an efficient technique to determine the structure and stability of native defects in crystalline silicon. Based on this combined approach, the growth behaviour of self-interstitial defects in crystalline Si is presented. New stable structures for small interstitial clusters (I_n, $5 \leq n \leq 16$) are determined and show that the compact geometry appears favoured when the cluster size is smaller than 10 atoms ($n < 10$). The fourfold-coordinated dodeca-interstitial (I_{12}) structure with C_{2h} symmetry is identified as an effective nucleation centre for larger extended defects. This work provides the first theoretical support for earlier experiments that suggest a shape transition from compact to elongated structures around $n = 10$. We also provide some theoretical evidence that suggests that {3 1 1} extended defects grow slowly along ⟨2 3 3⟩ and relatively faster along ⟨1 1 0⟩, which is consistent with typical defect aspect ratios observed through transmission electron microscopy.

Keywords: integrated atomistic modelling; interstitial defect growth; crystalline silicon

1. Introduction

Self-interstitials and vacancies are fundamental native defects in all crystalline materials. Ballistic processes that occur during high-energy ion implantation during semiconductor manufacturing, lead directly to a local vacancy excess at a depth nearly half the projected ion range and a silicon interstitial excess distribution at a depth close to the ion range [1,2]. It is well established that single interstitials and single vacancies are highly mobile in Si, even at room temperature [3–7], allowing the excess interstitials and vacancies to remain in bulk Si in the form of clusters or complexes with injected dopants. The formation and structure of rod-like {3 1 1} defects have been well characterised by high-resolution transmission electron microscopy [8–10]. In addition, a series of recent spectroscopy measurements [11–16] have evidenced the existence of small compact self-interstitial clusters before they evolve into larger extended defects. Earlier experiments based on gold labelling [17,18] and positron annihilation [19,20] also evidenced the existence of small vacancy clusters. Upon annealing at high temperatures, large open volume defects (greater than a few nanometres in diameter) were detected by transmission electron spectroscopy [21–24].

There have been significant efforts to understand the fundamental behaviour of these native defects as a consequence of their crucial role in defining ultrashallow pn junctions for ever-smaller semiconductor device fabrication. In ultrashallow junction formation with low-energy implanted dopants, such small native defect clusters are thought to be a main source for free interstitials and vacancies responsible for dopant transient enhanced diffusion and agglomeration during post-implantation thermal treatment [25–43]. Hence, significant experimental and theoretical efforts [44–70] have been made to determine the structure and stability of small native defect clusters as well as their growth mechanism to form larger extended or open volume defects. While the empirical studies are rather limited to show explicitly the formation and atomic structure of small defect clusters, a few small defect clusters have been unequivocally identified by first principles calculations [45,47,48, 50,55]. However, the atomic structure and stability of larger defect clusters cannot be determined using first principles calculations alone, largely due to the possible complexity in their geometries. This lack of information impedes the understanding of how small defect clusters evolve into larger ones.

First principles calculation efforts have revealed that native defect clusters tend to be fourfold-coordinated as the cluster size increases [47,48,55]. This led us to develop an integrated modelling strategy that combines continuous random network model-based Metropolis Monte Carlo (CRN-MMC), tight-binding molecular dynamics (TBMD) and density functional theory (DFT) calculations. Using this combined approach, we have recently provided extensive theoretical support for the growth and structural evolution of Si self-interstitial and vacancy clusters in Si [71–73]. In this paper, we introduce our recent work on the growth behaviour of self-interstitial Si clusters.

*Corresponding author. Email: gshwang@che.utexas.edu

ISSN 0892-7022 print/ISSN 1029-0435 online

DOI: 10.1080/08927020902929802
http://www.informaworld.com

2. Computational approach

Within the CRN model [74], a disordered structure is generated via a large number of bond transpositions using MMC sampling. The CRN-MMC approach has been successfully used to determine the fully relaxed structure of amorphous materials and their interfaces, while MD simulations alone may not always guarantee the construction of thermally equilibrated structures due to their intrinsic time scale limitations. Likewise, we expect that the structure of self-interstitial clusters in Si can also be predicted using CRN-MMC simulations, if all atoms in the clusters are fourfold-coordinated. The CRN-MMC approach will certainly be inadequate to determine the structure of defect clusters with a number of coordination defects. According to recent theoretical studies [47,55], however, the fourfold-coordinated structure of self-interstitial clusters of size n in Si appears energetically favoured when they are sufficiently large ($n \geq 3$). Apparently, the trade-off of energy gain via bond formation generally exceeds the strain energy arising from the fourfold coordination of clusters.

We employed Keating-like potentials [75] that have been proven to be reliable for determining the relaxed structure of disordered Si materials. Within the Keating-like valence force model, the strain energy (E_{strain}) is defined as

$$E_{\text{strain}} = \frac{1}{2}\sum_{i} k_{\text{b}}(b_i - b_0)^2 + \frac{1}{2}\sum_{i,j} k_{\theta}(\cos\theta_{ij} - \cos\theta_0)^2, \tag{1}$$

where the first and second terms on the right hand side show changes in the strain energy arising from deviations in bond lengths and bond angles, respectively, from their equilibrium values; b_i and b_0 represent the ith bond length and the equilibrium value, respectively; θ_{ij} is the bond angle between bonds i and j to a common atom with the equilibrium value of θ_0; and k_{b} and k_{θ} are force constants for the two-body and three-body interactions, respectively.

The potential parameters were optimised based on first principles DFT calculations. First, the two-body force constant (k_{b}) was adjusted to fit DFT values for the total energy variation of crystalline Si with varying amounts of strain (from 10% compressive to 10% tensile). Then, the three-body force constant (k_{θ}) was adjusted to fit DFT values for the strain energies of five different amorphous Si model structures (of each is within a 64-atom simple cubic cell). Finally, the values for k_{b} and k_{θ} were further refined simultaneously based on several interstitial clusters, such as I_4, I_7 and I_8. Through such thorough optimisation, we have obtained a set of parameters, $k_{\text{b}} = 11.976\,\text{eV/Å}^2$ and $k_{\theta} = 2.097\,\text{eV}$, for DFT values of $b_0 = 2.364\,\text{Å}$ and $\theta_0 = 109.5°$. Note that the optimised parameters are somewhat different from those available

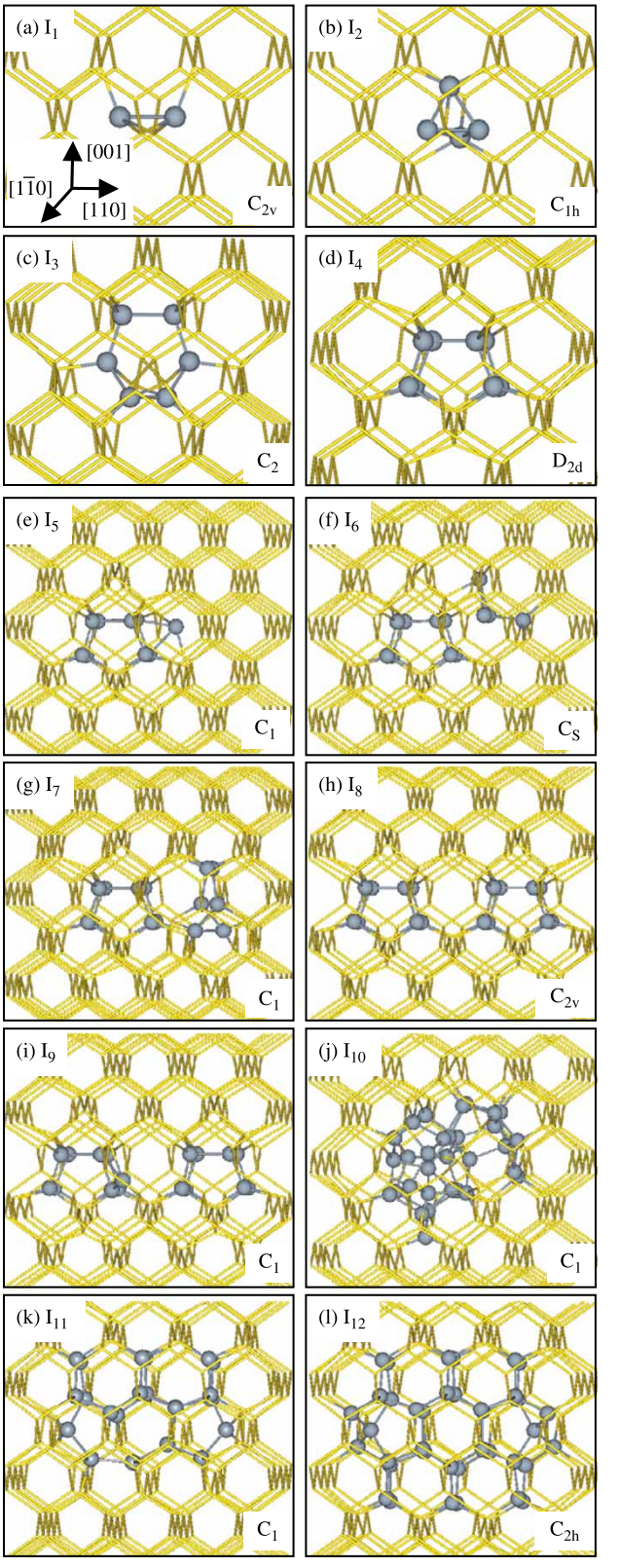

Figure 1. (Colour online) Minimum energy configurations for small self-interstitial defects (I_n, $n \leq 12$) in the neutral state with corresponding defect symmetries indicated in Si. Grey balls indicate more distorted atoms than the rest of the light grey (gold)

in the literature ($b_0 = 2.35$ Å, $\theta_0 = 109°$, $k_b = 9.08$ eV/Å^2, and $k_\theta = 3.57$ eV) [75].

Using the CRN-MMC approach, we first determined possible fourfold-coordinated structures for interstitial clusters of different sizes (I_3–I_{10}), starting with various initial seed configurations for each case. The thermal stability of the fourfold-coordinated model structures was checked using TBMD based on highly optimised semi-empirical potentials developed by Lenosky et al. [76]. The structures and energetics of the stable clusters determined by combined CRN-MMC and TBMD simulations were further refined using first principles calculations based on DFT within the generalised gradient approximation of Perdew and Wang (GGA-PW91) [77]. While the CRN-MMC, TBMD or DFT methods alone are likely limited to sample all possible cluster configurations, the combined approach has proven itself an effective procedure to determine the complex minimum energy states of small self-interstitial clusters in Si.

All atomic structures and energetics reported herein were calculated using the well-established planewave program Vienna *ab initio* simulation package (VASP) [78]. For DFT-GGA calculations, the supercell lattice constants were fixed at 5.460 Å, as obtained from careful volume optimisation. A planewave cut-off energy of 160 eV was used. Vanderbilt ultrasoft pseudopotentials [79] for core-electron interactions were employed and Brillouin zone sampling was performed using Monkhorst–Pack type k-point meshes. The mesh size was set to $(2 \times 2 \times 2)$ for the 216 atom simple cubic supercell and was scaled with supercell size. For each defect system, all atoms were fully relaxed using the conjugate gradient method until residual forces on constituent atoms became smaller than 5×10^{-2} eV/Å.

3. Results and discussion

3.1 Determination of stable fourfold interstitial clusters

For comparison, we first determined the lowest energy configurations of the mono-, di-, tri- and tetra-interstitial clusters in their neutral charge states. Our calculations show the ground state split-$\langle 1\,1\,0\rangle$, C_{1h}, C_2 and D_{2d} symmetry structures for I, I_2, I_3 and I_4, respectively, as also predicted by previous theoretical studies [50,55]. It is worth emphasising that our CRN-MMC calculations consistently predict the fourfold-coordinated C_2 and D_{2d} configurations for I_3 and I_4, respectively, as shown in Figure 1, regardless of the initial interstitial positions as long as they are in close proximity. This indicates the effectiveness of the CRN-MMC approach for determining fourfold defect structures in which all atoms have fourfold coordination.

Figure 1 also shows minimum energy structures that we have identified for I_5 through I_{12} using a combination of CRN-MMC, TBMD and DFT-GGA calculations. For each cluster size, we first constructed possible fourfold-coordinated structures using CRN-MMC simulations, followed by TBMD simulations at high temperatures (>1000 K), to check their thermal stability. Then, we used DFT-GGA calculations to refine the geometries of the identified stable clusters and compared their formation energies to determine the lowest energy configuration among them. The combined approach has proven successful in determination of minimum energy configurations for Si self-interstitial clusters (I_n, $n \geq 3$), particularly when they prefer fourfold coordination [71]. In this work, we only present the lowest energy state for each cluster size among several local minima identified from our extensive search. Other stable structures can be found elsewhere [71].

Our results show that small interstitial clusters tend to favour compact structures, but the compact geometry is no longer favourable when the cluster size exceeds 10 interstitials. All atoms in the hendeca-interstitial [I_{11}; Figure 1(k)] and dodeca-interstitial [I_{12}; Figure 1(l)] clusters are fourfold-coordinated and they are elongated along the [1 1 0] direction. While the I_{11} cluster exhibits a somewhat asymmetric shape, the I_{12} structure is perfectly symmetric and less strained. The I_{12} structure has mirror symmetry with respect to the (1 1 0) plane (perpendicular to the C_2 rotation axis along the [1 1 0] direction). Having four interstitials in each unit, the core part [see also Figure 6(a)] is characterised by four adjacent six-membered rings surrounded by five-, six- and seven-membered rings. The (1 1 0) surface atoms are also fourfold-coordinated and their bond angles and lengths range from 98.8° to 128.2° and from 2.243 to 2.348 Å, respectively. Both parameters deviate insignificantly from their respective equilibrium values of 109.5° and 2.365 Å in crystalline Si. The I_{12} formation energy is predicted to be 1.60 eV per interstitial, which is substantially lower than 3.80 eV for the split-$\langle 1\,1\,0\rangle$ mono-interstitial.

We also find that the octa-interstitial (I_8) cluster (comprising two stable compact I_4 clusters) is very stable. For the minimum energy I_8 configuration, two complete I_4 core structures are adjacent along the [1 1 0] direction, as shown in Figure 1(h). The I_4–I_4 alignment with C_{2v} symmetry yields two eight-membered rings in the interface region, which turns out to lower the induced strain relative to two isolated I_4 core clusters. While there is an energy variation as the I_4–I_4 alignment within the Si lattice changes [71], the predicted ground state structure of I_8 is about 0.71 eV more favourable than the case, where two I_4 clusters are fully separated.

wireframe lattice. Light grey (gold) wireframe represents the bulk Si lattice. Dark grey spheres represent interstitial atoms and their highly strained neighbours.

As a consequence of the high thermal stability of the I_4 and I_8 structures, the penta-interstitial [I_5; Figure 1(e)] and ennea-interstitial (I_9) clusters [Figure 1(i)] favour the $I_4 + I$ and $I_8 + I$ configurations, respectively, where the additional single interstitial is located near their host I_4 or I_8 cluster. For the hexa-interstitial [I_6; Figure 1(f)] and hepta-interstitial (I_7) clusters [Figure 1(g)], the combined $I_4 + I_2$ and $I_4 + I_3$ configurations appear energetically favoured with energy gains of 1.16 and 0.37 eV, respectively, over their fully-separated counterparts (isolated I_2, I_3 or I_4 clusters). Similarly, a stable $I_8 + I_2$ configuration is identified for the deca-interstitial (I_{10}) cluster, but turns out to be 0.36 eV less favourable than the stable fourfold-coordinated structure as shown in Figure 1(j). Our calculations also predict the $I_8 + I_3$ [Figure 2(a)] and $I_8 + I_4$ [Figure 2(b)] structures to be 0.93 and 1.59 eV less stable than the elongated, fourfold-coordinated I_{11} and I_{12} structures, respectively.

3.2 *Compact-to-elongated transition*

Figure 3 summarises both the calculated formation energies of small interstitial clusters and several configurations of elongated structures. Here, the formation energy per interstitial [$E_f(n)$] is given by

$$E_f(n) = (E(n+N) - (1 + n/N) \times E(N))/n, \qquad (2)$$

where $E(n + N)$ and $E(N)$ are the total energies of N-atom supercells with an I_n cluster and without defect, respectively. The predicted E_f values of 3.80, 2.79, 2.06 and 1.85 eV, respectively, for the I, I_2, I_3 and I_4 clusters are in good agreement with previous DFT-GGA calculations [50,55]. The predicted formation energies exhibit an oscillating trend as the cluster size varies, with strong minima at $n = 4$ and 8, consistent with inverse modelling experiments [80,81]. Based on these calculations, we discuss the nucleation and growth of large, extended defects by evaluating three proposed models.

Prior to our study, the presence of stable, chain-like, elongated, interstitial clusters Figure 4 for $n \geq 3$ was reported by Kim et al. [52]. These chain-like configurations are extended by concatenating dumbbell-like split-$\langle 1\,1\,0 \rangle$ interstitials to the existing core structure. While the fourfold compact cluster was identified to be more stable than the chain-like, elongated cluster at $n = 4$, this study did not report the existence of larger compact clusters based on the I_4 core that have lower energy configurations than the chain-like, elongated clusters. At the time, the existing calculations led to the conclusion that small compact clusters may evolve into chain-like, elongated clusters for $n \approx 5$–8. This model of the compact-to-extended structural growth transition mechanism

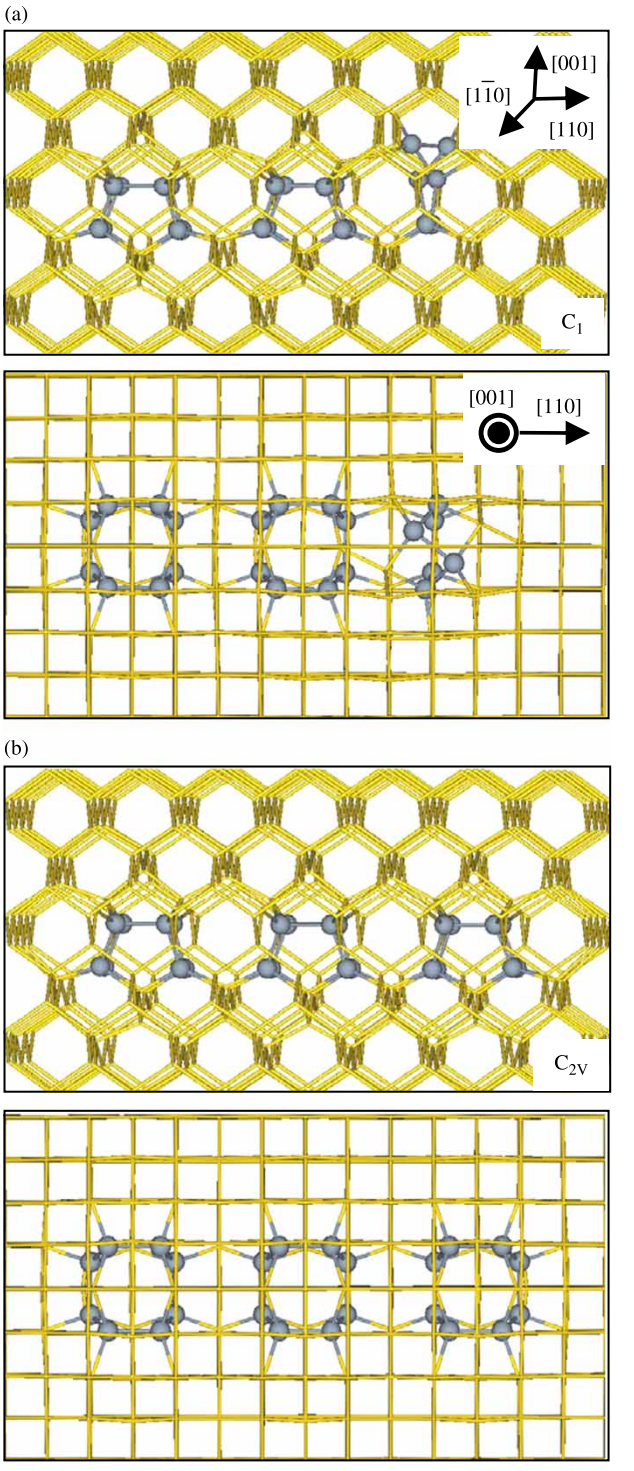

Figure 2. (Colour online) Compact, minimum energy configurations with corresponding defect symmetries for (a) hendeca- and (b) dodeca-interstitial defects in Si. For each defect, the top and bottom panels show two different views, as indicated. Light grey (gold) wireframe represents the bulk Si lattice. Dark grey spheres represent interstitial atoms and their highly strained neighbours.

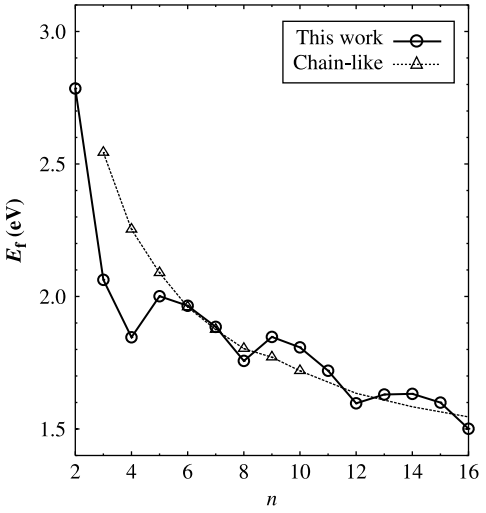

Figure 3. Calculated formation energies per interstitial (E_f) for interstitial clusters shown in Figures 1 and 5 (indicated as 'This work') as well as chain-like elongated structures (indicated as 'Chain-like') configurations, and {311} core structures as a function of cluster size (n). For the chain-like case, the atomic structures of Kim et al. [52] were recalculated within DFT-GGA. To minimize possible interactions between a defect and its periodic images, we evaluated the formation energies by scaling the supercell size as follows ('This work'): $192 + n$ (I_1–I_2), $400 + n$ (I_3–I_6), $480 + n$ (I_7–I_{10}), $560 + n$ (I_{11}–$_{13}$), and $672 + n$ (I_{14}–I_{16}) atom supercells, where n is the number of interstitials. Likewise, the following supercells sizes were used ('Chain-like'): $400 + n$ (I_3–I_4), $480 + n$ (I_5–I_6), $560 + n$ (I_7–I_8), and $640 + n$ (I_9–I_{10}) atom supercells. For $n > 10$, the chain-like cluster formation energy is forecasted using $E_f(n) = \{6.83 + (n - 2) \times 1.28\}/n$, see also Figure 9.

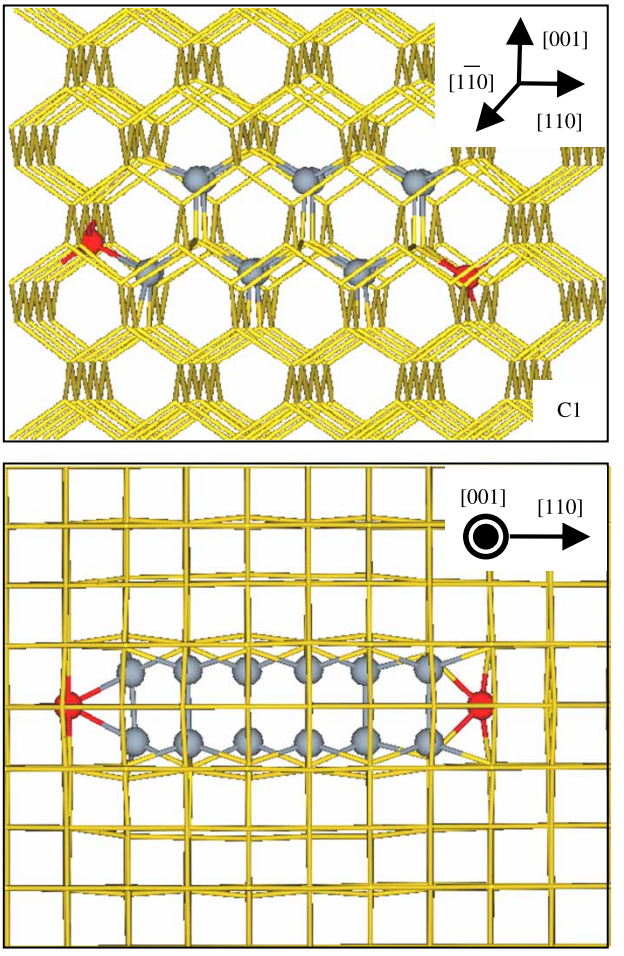

Figure 4. (Colour online) Configuration for the chain-like, elongated hexa-interstitial defect with C_1 symmetry in Si. The top and bottom panels show two different views, as indicated. Dark grey (red) balls indicate highly distorted atoms in the (110) interfaces, grey balls represent interstitial atoms and their highly strained neighbors, and light grey (gold) wireframe represents the bulk Si lattice.

proposed the chain-like, elongated tri-interstitial cluster as a key component and seed for extended structure growth [52,55].

Our recent studies using the combined computational approach have shown that the compact configurations are comparable or more stable than the chain-like, elongated clusters for $n \leq 8$, as shown in Figure 4. Our results also suggest that the transition from compact to well-ordered chain-like configurations would be difficult because the compact I_4 core structure is relatively very stable. Our TBMD simulation at 1100 K shows that the $I_4 + I$ structure remains nearly unchanged for 20 ps, whereas the compact I_3 ground state cluster easily collapses when it captures an additional interstitial and would further reconfigure itself into the stable I_4 core structure. This behaviour suggests that the stable I_4 and I_8 compact clusters would kinetically and/or thermodynamically deter the formation of small chain-like clusters ($n \leq 10$).

For $n > 10$, the elongated configuration becomes more stable than the compact shape. The elongated configuration generally has strained {1 1 0} terminating surfaces or interfaces. This excess strain energy deters chain-like, elongated configurations for small n, but the terminating surface effects are diminished as n increases. This observation suggests that fourfold compact clusters may evolve into chain-like, elongated structures for $n \approx 10$ and further growth may occur by the capture of interstitials at the strained {1 1 0} terminating surfaces.

Another plausible transition growth mechanism may involve the elongated, fourfold I_{11} and I_{12} clusters identified in our work. In the size regime, where $n > 10$, we do not anticipate interconversion between the elongated, fourfold-coordinated clusters we have presented and the chain-like, elongated configurations proposed by Kim et al. because of the well-ordered structure and high thermal stability exhibited by the elongated fourfold-coordinated clusters.

Figure 5 (upper right panel) shows an atomic-level strain distribution profile for the fourfold I_{12} cluster based on

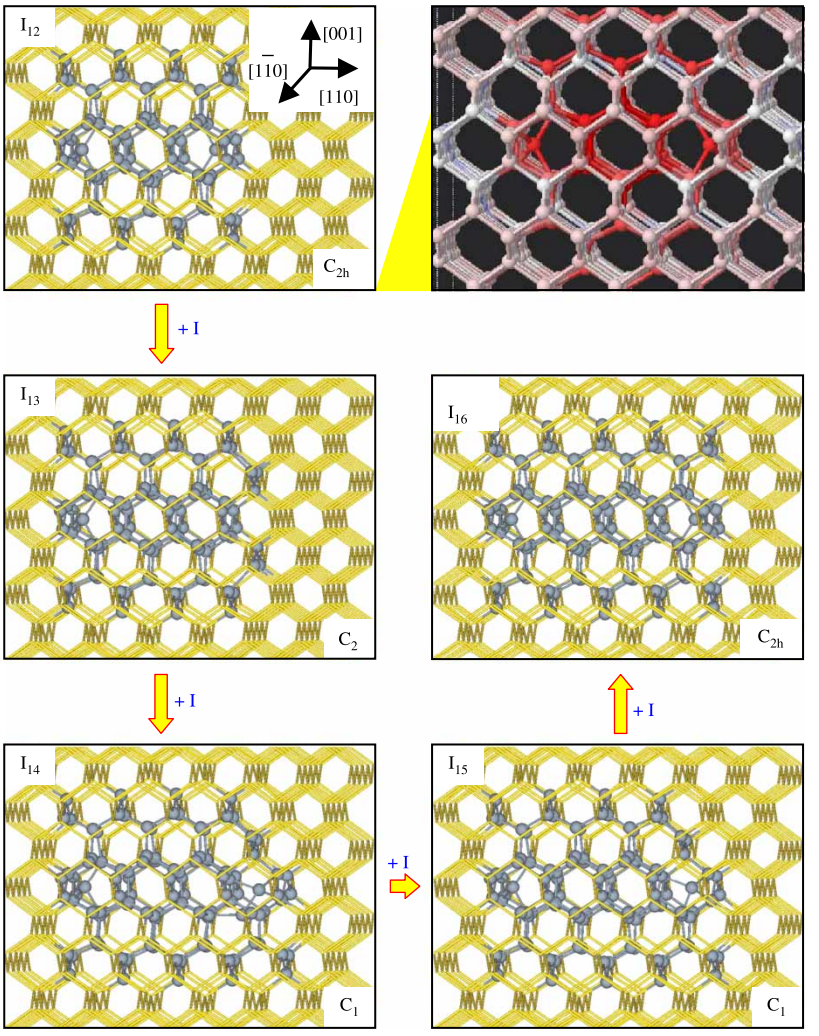

Figure 5. (Colour online) Minimum energy structures for I_{12} through I_{16} with the I_{12}-like core, which exhibit preferred growth along the [1 1 0] direction when $n > 10$. Configurations for I_{12} through I_{16} are depicted with dark grey balls showing highly distorted atoms and light grey (gold) wireframe representing the bulk lattice. Additionally, the upper right panel provides an atomic-level strain distribution profile for the I_{12} cluster and nearby bulk Si based on average bond length. Each atom is assigned an average bond length based on the four bonds formed with its nearest neighbours and is gradient-shaded accordingly. The colour spectrum shifts from red to white to blue (RWB) as the average bond lengths shift from compressive to strain-free to tensile. The RWB spectrum range displayed here covers the Si–Si DFT equilibrium bond length of 2.36 ± 0.07 Å.

average bond lengths. The colour of each atom is gradient-shaded according to the average bond length shared with its four neighbours. Compressive strain is indicated by red, strain-free is white, and tensile strain appears as blue. Larger strain is seen near the (1 1 0) interfaces, indicating that they are more active than the {3 1 1} and {2 3 3} interfaces. Our TBMD simulations indeed demonstrate that an additional interstitial placed around the I_{12} cluster is preferentially captured at the (1 1 0) interfaces, as defined, to form the I_{13} cluster. Additionally, Figure 5 reveals the minimum energy fourfold configurations of the I_{14}, I_{15} and I_{16} clusters during the proposed growth sequence from the I_{12} configuration. The I_{13}, I_{14}, I_{15} and I_{16} formation energies per interstitial are predicted to be 1.63, 1.63, 1.60 and 1.50 eV, respectively. Note that the I_{16} structure with C_{2h} symmetry is an extension of I_{12} with an additional core unit added in the [1 1 0] direction. By capturing additional interstitials, the interstitial defect structure grows preferentially along the [1 1 0] direction. This behaviour suggests that I_{12} can serve as an effective nucleation seed for the growth of larger extended defects.

3.3 *Growth to {3 1 1} extended defects*

We also examined the possible evolution of small, fourfold and chain-like, elongated clusters into extended defects with a {3 1 1} habit plane. In Figure 6, we compare the I_{12}-like core structure [Figure 6(a)] previously detailed

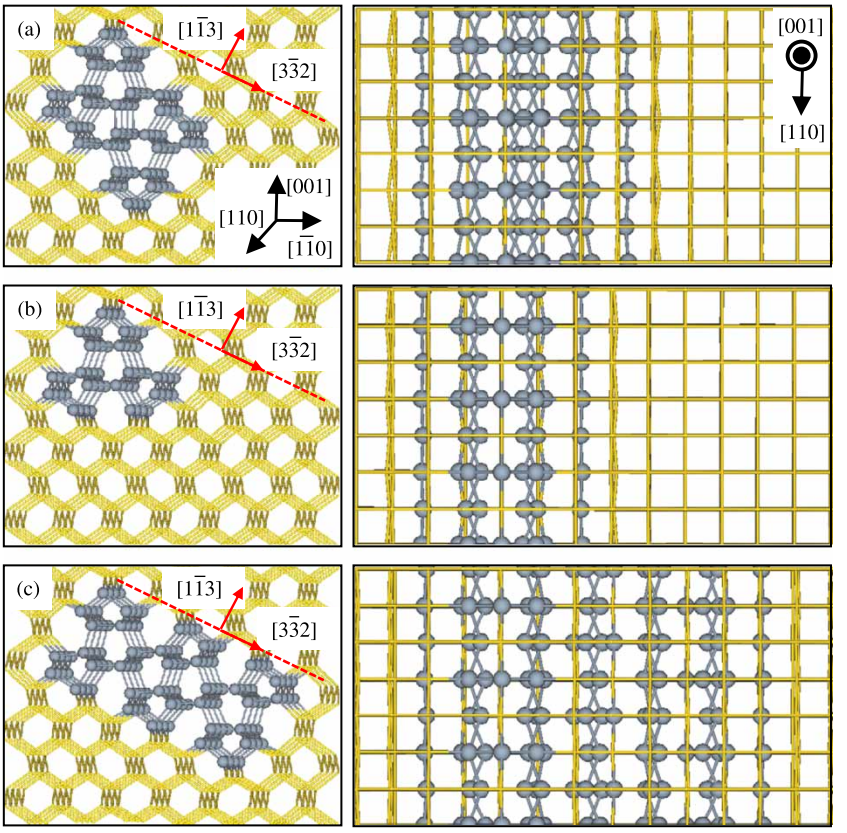

Figure 6. (Colour online) Three different defect core structures that are infinitely long in the [1 1 0] direction: (a) I_{12}-like (as shown for the fourfold I_{12} cluster identified in this work); (b) chain-like and (c) {3 1 1}. For each core, the left and right panels show two different views, as indicated. Grey balls indicate more distorted atoms than the rest of the light grey (gold) wireframe lattice.

in Figure 5, the chain-like, elongated core structure [Figure 6(b)] of Kim et al., and a plausible {3 1 1} core structure [Figure 6(c)]. In Figure 6, all three defect cores shown are cross-sections that effectively extend infinitely in the [1 1 0] direction using periodic boundary conditions of the supercell method. The {3 1 1} core consists of four six-membered rings in the middle layer and six five- and six seven-membered rings in the outer layers, as proposed by earlier studies [82–84]. Other {3 1 1} core configurations have also been predicted [52,82–85], but the most favourable structural sequence is still undetermined. We feel our conclusions are general enough that our observed results of the interaction between small interstitial clusters and the exemplary {3 1 1} structure in Figure 6(c) can be applied to other plausible {3 1 1} defect structures.

For each repeating unit of the structures shown in Figure 6, the I_{12}-like and {3 1 1} cores contain four interstitials, while the chain-like, elongated structure has only two. The I_{12}-like core has a higher interstitial density than either the chain-like or {3 1 1} cores. Compared to the I_{12}-like core, the chain-like core must be twice as long along [1 1 0] and the {3 1 1} core must be twice as long along [3 $\bar{3}$ 2] to match the number of net embedded interstitials. The I_{12}-like and {3 1 1} cores both exhibit a representative fraction of the {3 1 1}-habit plane, but the chain-like, elongated structure does not. In addition, transformation from the I_{12}-like to {3 1 1} core is plausible via structural relaxation along the ⟨2 3 3⟩ direction. However, it appears unlikely that the chain-like, elongated core of Figure 6(b) could reconfigure into the {3 1 1} core of Figure 6(c) because the chain-like configuration contains two less net interstitials per unit length along the ⟨1 1 0⟩ direction. The required structural transformation to convert the chain-like core of Figure 6(b) into the {3 1 1} core of Figure 6(c) would need the chain-like configuration to compress by 50% along ⟨1 1 0⟩ while simultaneously stretching by 100% along ⟨2 3 3⟩. This type of physical transformation on an extended scale is improbable. The less dense {3 1 1} core has a lower E_f than the I_{12}-like core, which suggests that the {3 1 1} core is more relaxed than the I_{12}-like core. The predicted formation energies of the {3 1 1}, I_{12}-like and chain-like, elongated cores are 1.11, 1.29 and 1.28 eV, respectively, assuming the cores are infinitely long in the [1 1 0] direction, as depicted in Figure 6. Our results reinforce the possibility of a compact-to-elongated transition mechanism initiated from fourfold-coordinated, elongated I_{11} and I_{12} clusters. This conclusion is consistent with

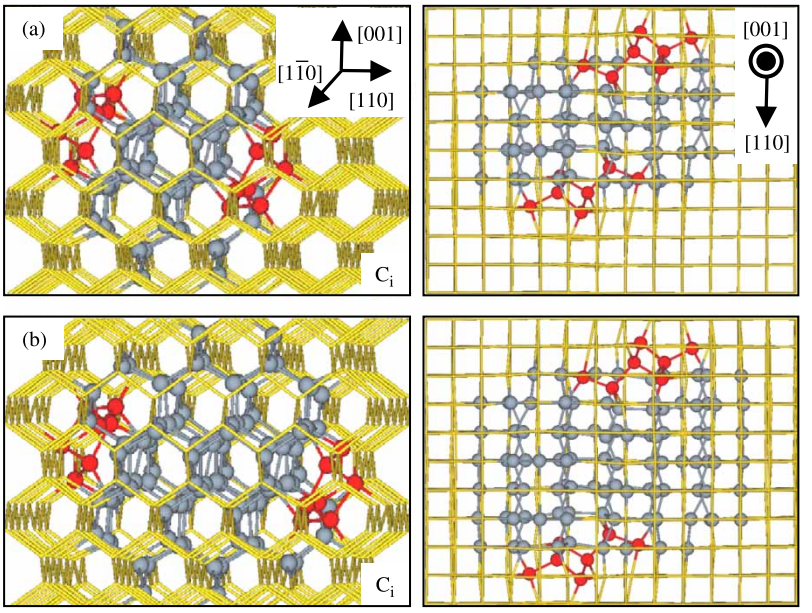

Figure 7. (Colour online) Minimum energy configurations for {3 1 1} core structures of (a) I_{12} and (b) I_{16} clusters in Si. For each defect, the left and right panels show two different views, as indicated. The symmetry of each defect is also indicated. Dark grey (red) balls indicate highly distorted atoms in the (1 1 0) interfaces, grey balls represent moderately distorted atoms and light grey (gold) wireframe represents the bulk Si lattice.

earlier experimental results, which suggested the incipience of a compact-to-elongated transition for $n \approx 10$ [80,81].

We also compared the relative stability of both the I_{12} [Figure 7(a)] and I_{16} [Figure 7(b)] clusters with the {3 1 1} core configuration, since the {3 1 1} core is energetically more favourable than the I_{12}-like core. As shown in Figure 8(c), the (1 1 0) interfaces can be fourfold-coordinated for the {3 1 1} core structure, even though each surface initially contains two dangling bonds. The fourfold coordination lowers the E_f of I_{12} by 1.1 eV over the initial structure with dangling bonds. Using CRN-MMC simulations, we also confirmed that the fourfold interfaces can favourably evolve for larger clusters with a {3 1 1} core configuration; however, we find that the (1 1 0) interface configuration is more strained for the {3 1 1} core than for the I_{12}-like core [Figure 8(a)]. Our calculations predict the {3 1 1} core structures (with C_i symmetry) to be 1.4 and 0.8 eV less favourable than the I_{12}-like core containing I_{12} and I_{16} clusters, respectively.

Figure 9 also compares the relative stability of large clusters with the I_{12}-like, chain-like and {3 1 1} cores, which we approximate using

$$E_f(n) = \{E_f^{end} + (n - n')E_f^c\}/n, \qquad (3)$$

where E_f^{end} is the {1 1 0} interface energy, E_f^c is the core energy per interstitial for the semi-infinite elongated structure, and n' represents the number of (1 1 0) interface terminating atoms. For the I_{12}-like and {3 1 1} cores, we use the core formation energies of $E_f^c = 1.29$ and 1.11 eV to estimate the corresponding (1 1 0) interface energies as $E_f^{end} = 8.74$ and 11.62 eV, respectively. Note that both cases have four (1 1 0) interface atoms ($n' = 4$). Similarly, for the chain-like, elongated core, we obtain $E_f^c = 1.28$ eV and $E_f^{end} = 6.83$ eV, where $n' = 2$ (the chain-like structure has two (1 1 0) interface atoms). From this result, the {3 1 1} core structure becomes most favourable for $n \geq 20$ atoms, while the I_{12}-like core should prevail for $n < 20$ atoms. This supports a possible structural relaxation from the I_{12}-like to {3 1 1} core structure near the $n \approx 20$ size regime as the interstitial cluster grows along the [1 1 0] direction.

Experimentally observed {3 1 1} defects are typically as long as 1 μm along the ⟨1 1 0⟩ direction and range from 1 to 100 nm in width along the ⟨2 3 3⟩ direction. Note that the ⟨2 3 3⟩ direction is perpendicular to the ⟨1 1 0⟩ and ⟨3 1 1⟩ directions as shown in Figure 10. This implies that a {3 1 1} defect gradually expands along the ⟨2 3 3⟩ direction while it quickly elongates along the ⟨1 1 0⟩ direction as it incorporates more interstitials during a thermal annealing process. This is shown schematically in Figure 10. We also constructed an extended defect with a {3 1 1} habit plane by adding repeating units to the {3 1 1} core of Figure 6(c) along the ⟨2 3 3⟩ direction. The predicted E_f per interstitial is significantly lower than the {3 1 1} core structure in Figure 8(c) with $E_f(\infty) = 0.89$ eV, which is in good agreement with expectations of 0.7–1.4 eV as reported for extended {3 1 1} defects in previous studies [86].

Finally, we briefly discuss the predicted growth behaviour along the ⟨2 3 3⟩ direction based on our

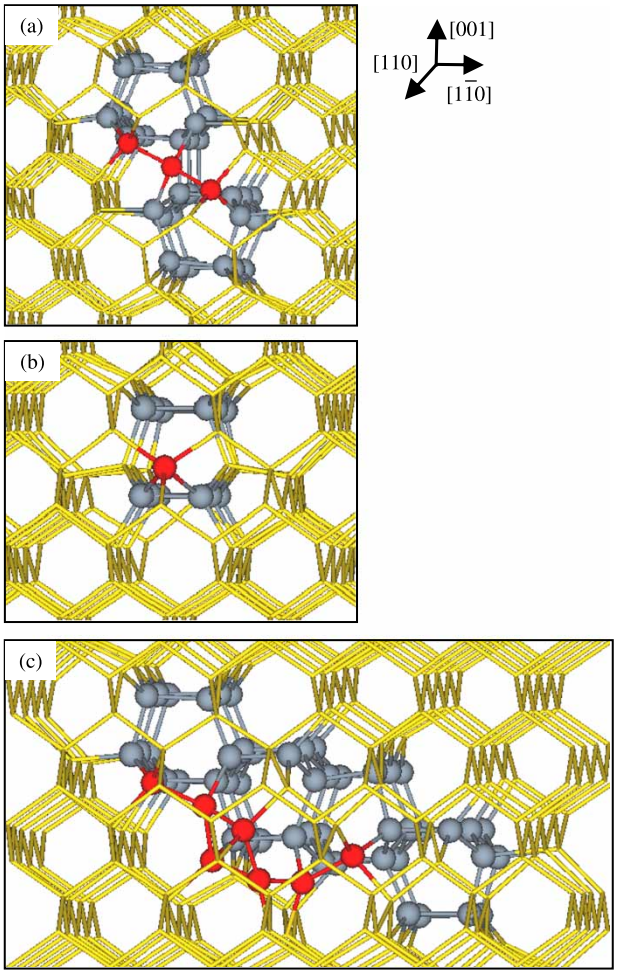

Figure 8. (Colour online) Minimum energy configurations for the (1 1 0) edges of (a) the elongated I_{12}-like, (b) chain-like and (c) {3 1 1} core configurations. Dark grey (red) balls indicate highly distorted atoms contained in the (1 1 0) interfaces, grey balls represent moderately distorted atoms and light grey (gold) wireframe represents the bulk Si lattice.

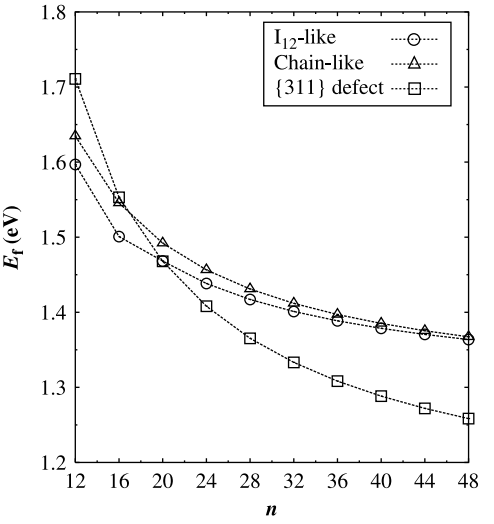

Figure 9. Predicted formation energies per interstitial of I_{12}-like, chain-like and {3 1 1} core configuration clusters as a function of size (n) using $E_f(n) = \{E_f^{end} + (n - n')E_f^c\}/n$, where E_f^{end} is the (1 1 0) interface energy; E_f^c is the core energy per interstitial for the semi-infinite structure; and n' is the number of interface atoms. Here, the interface energies were obtained by numerically fitting DFT-GGA values for the formation energies of small clusters: I_{12} and I_{16} were used for the I_{12}-like and {3 1 1} cases, while I_8, I_9 and I_{10} represented the chain-like, elongated structures. The predicted values are based on $E_f^c = 1.29$, 1.28 and 1.11 eV and $E_f^{end} = 8.74$, 6.83 and 11.62 eV for the I_{12}-like, chain-like and {3 1 1} cases, respectively. For the number of interface atoms, $n' = 4$ was used for the I_{12}-like and {3 1 1} structures, while $n' = 2$ was used for the chain-like, elongated structure.

preliminary results. Figure 11(a) exhibits an atomic-level strain distribution profile throughout the model {3 1 1} core structure using the same parameters as Figure 5 (upper right panel). According to our analysis, the (3 $\bar{3}$ 2) interface is under tensile strain (blue), while the (1 $\bar{1}$ $\bar{3}$) interface is under mild compressive strain (pink), which is consistent with a previous theoretical study [84]. Strain distributions from all extended defects with a {3 1 1} habit plane we studied show a similar trend. This indicates that additional interstitials, which generally induce a localised compressive strain field, are more likely to aggregate at the (3 $\bar{3}$ 2) tensile interface to quench strain rather than at the (1$\bar{1}\bar{3}$) compressive interface.

To verify this potential interstitial growth mechanism influenced by the local strain field, we added additional interstitials near an extended defect with a {3 1 1} core. Our CRN-MMC simulations clearly show that the interstitials preferentially append to the extended defect at the (3 $\bar{3}$ 2) interfaces, as shown in Figure 11. In Figure 11(b), three additional interstitials form a stable tri-interstitial cluster whose configuration is similar to the ground state I_3 cluster. The appended tri-interstitial cluster is

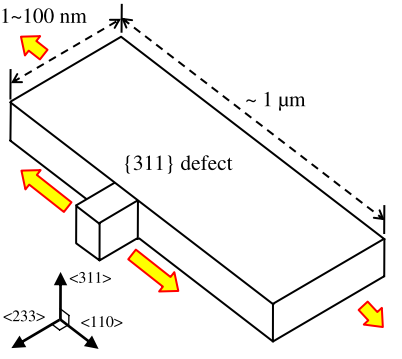

Figure 10. Block diagram for a typical {3 1 1} extended defect structure. Characteristic dimensions observed experimentally and alignment of the defect within the bulk Si lattice is shown. From the computational results obtained, incremental growth along ⟨2 3 3⟩ (small block extension) followed by more favourable growth along ⟨1 1 0⟩ (block arrows) is anticipated.

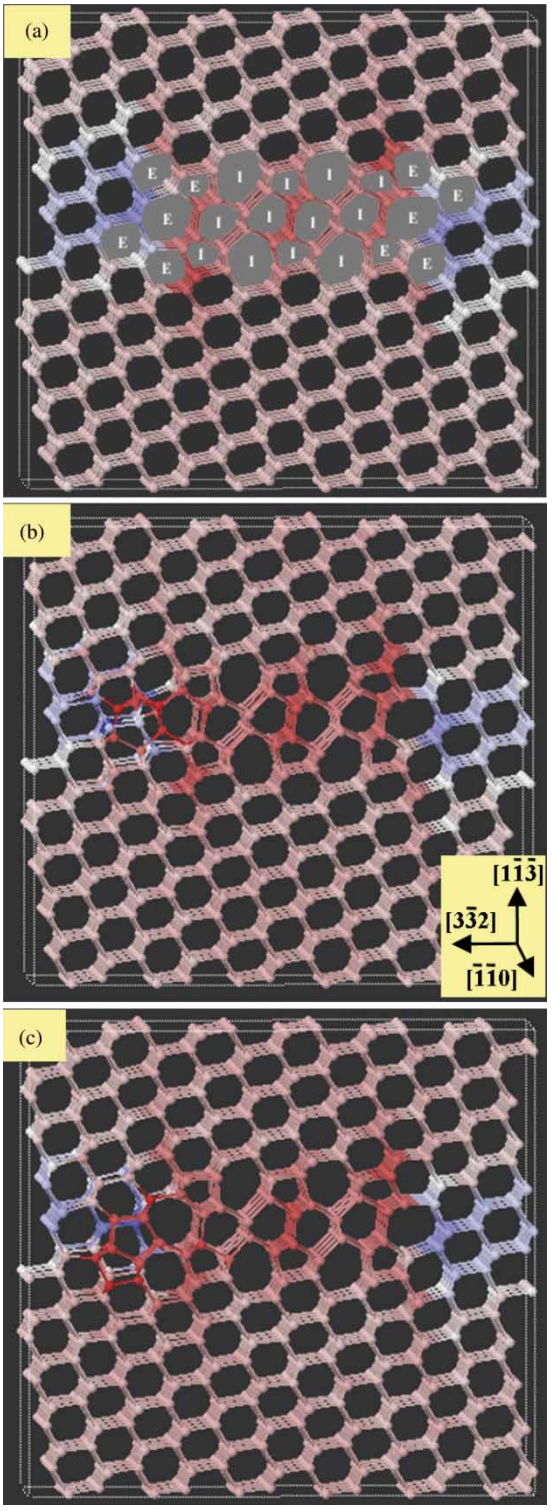

Figure 11. (Colour online) (a) An atomic-level strain distribution profile throughout the {3 1 1} core structure and nearby bulk material based on average bond length. Each atom is assigned an average bond length based on the four bonds formed with its nearest neighbours and is gradient-shaded accordingly. The colour spectrum shifts from RWB as the average bond lengths shift from compressive to strain-free to tensile. The RWB spectrum range displayed here covers the Si–Si DFT equilibrium bond length of 2.36 ± 0.07 Å. Additionally, the constituent rings of the model {3 1 1} core have been shaded grey to help visualise the defect cross-section in the bulk. The 'I' (interstitial) and 'E' (edge) ring annotations reflect the nomenclature of Kohyama and Takeda [82] to generalise the periodicity seen in {3 1 1} planar structures. From left to right, this structure would be labelled 'EIIE'. The 'I' repeating unit contains two net interstitials per period along ⟨1 1 0⟩. From the strain profile, the structure core is compressively strained, the {3 1 1} interface planes are under slight compression, and the {2 3 3} interface planes are under tensile strain. Minimum energy configurations for (b) '{3 1 1} core + I_3' and (c) '{3 1 1} core + I_4' structures. In both cases, the interstitials appended themselves to the tensile {2 3 3} interface to help minimise excess strain energy. The appended tri-interstitial and tetra-interstitial configurations (bright red) show strong resemblance to the ground state I_3 and I_4 compact configurations of Figure 1.

compressively strained, as indicated by the bright red colour. At the (3 $\bar{3}$ 2) interface, two five-membered rings of the ground state I_3 cluster combine with two seven-membered rings of the {3 1 1} core, resulting in two six-membered rings. Likewise, in Figure 11(c), four additional interstitials form a stable tetra-interstitial cluster that resembles the ground state I_4 cluster. Again, the appended tetra-interstitial cluster is compressively strained and appears bright red. At the (3 $\bar{3}$ 2) interface, two seven-membered rings of the ground state I_4 cluster combine with two seven-membered rings of the {3 1 1} core, resulting in two seven-membered rings. As a result, the hybrid '{3 1 1} core + I_3' and '{3 1 1} core + I_4' structures have binding energies of 1.1 and 1.2 eV with respect to the separated '{3 1 1} core + I_3' and '{3 1 1} core + I_4' component structures, respectively, according to our force field calculations. For comparison, we also identified the structure and stability of possible I_3 and I_4 clusters at the (1 $\bar{1}$ $\bar{3}$) interface plane. Unlike the clusters appended to the (3 $\bar{3}$ 2) interfaces, the I_3 and I_4 clusters do not yield similar structures to the ground state I_3 and I_4 clusters, respectively, when formed in the mildly compressive region along the (1 $\bar{1}$ $\bar{3}$) interface. As a consequence, the binding energies of the I_3 and I_4 clusters at the (1 $\bar{1}$ $\bar{3}$) interface were significantly lower than those at the (3 $\bar{3}$ 2) interface by 0.6 and 0.5 eV, respectively.

We also evaluated the addition of the small interstitial clusters near the ($\bar{1}$ $\bar{1}$ 0) interface of the {3 1 1} defect structure. We estimated the binding energy of the tetra-interstitial cluster (when it forms another repeating unit along the [$\bar{1}$ $\bar{1}$ 0] direction) at the ($\bar{1}$ $\bar{1}$ 0) interface as 2.5 eV, which is twice as large as the binding energy found at the (3 $\bar{3}$ 2) interface. Given the binding energy results of our work and the typical ratio of dimensions observed experimentally for extended {3 1 1} defect structures, it is reasonable to propose that the defect growth rate along ⟨1 1 0⟩ is the fastest, followed by the growth rate along

$\langle 2\,3\,3\rangle$, while the growth rate along $\langle 3\,1\,1\rangle$ should be the slowest.

As depicted by the block diagram in Figure 10, a possible multi-step mechanism is shown that integrates our computational results for extended defect growth. First, newly formed small compact cluster units append to the $\{2\,3\,3\}$ interfaces. Second, these new additional interstitial building blocks seed rapid chain growth along the $\langle 1\,1\,0\rangle$ direction. The eventual result is the extension of the $\{3\,1\,1\}$ defect in the $\langle 2\,3\,3\rangle$ dimension. We also propose the possibility of relatively highly strained small compact clusters playing a critical role as initiators for further structural relaxation of the already grown $\{3\,1\,1\}$ defect, ultimately leading to the formation of well-relaxed, extended defects with $\{3\,1\,1\}$ habit planes. Further, investigation is underway to understand the atomic-level mechanisms in silicon that drive $\{3\,1\,1\}$ defect growth in the $\langle 1\,1\,0\rangle$ and $\langle 2\,3\,3\rangle$ directions.

4. Summary

We have determined stable, compact geometries for small interstitial clusters ($n < 10$) and demonstrated that stable I_4 and I_8 compact clusters would kinetically or/and thermodynamically inhibit the formation of chain-like, elongated clusters. When the cluster size exceeds 10 atoms, our calculations show that elongated structures become more favourable energetically, although they commonly consist of highly strained $\{1\,1\,0\}$ interfaces, which make them less favourable configurations for smaller clusters. In particular, the newly discovered fourfold-coordinated I_{12} configuration is found to serve as an effective nucleation centre for larger extended defects. For the first time, this theoretical work provides explicit support for earlier experiments, which suggested the occurrence of the compact-to-elongated transition at $n \approx 10$. In addition, the predicted formation energies per interstitial generally decrease with cluster size, but also exhibit an oscillating trend with strong minima at $n = 4$ and 8, which is consistent with earlier inverse model studies based on experiment. While the fourfold I_{12}-like core is energetically less favourable than a typical $\{3\,1\,1\}$ defect core, our theoretical results suggest the possible occurrence of further structural relaxation from the I_{12}-like to $\{3\,1\,1\}$ core configuration as the cluster grows larger than $n \approx 20$ along the $\langle 1\,1\,0\rangle$ direction. We also propose the possible formation of compact interstitial clusters at the $\{2\,3\,3\}$ interfaces of extended $\{3\,1\,1\}$ defect structures driven by minimisation of local strain energy. These compact clusters formed at the $\{2\,3\,3\}$ interfaces can potentially seed further growth along the $\langle 1\,1\,0\rangle$ direction, ultimately leading to incremental growth along $\langle 2\,3\,3\rangle$ and more rapid growth along $\langle 1\,1\,0\rangle$ for extended $\{3\,1\,1\}$ defect structures. Our integrated modelling technique has many applications ranging from identification of small interstitial cluster configurations to prediction of the growth behaviour of extended defect structures.

Acknowledgements

We acknowledge Semiconductor Research Corporation (1413-001), National Science Foundation (CAREER-CTS-0449373) and Robert A. Welch Foundation (F-1535) for their financial support. We would also like to thank the Texas Advanced Computing Center for use of their computing resources.

References

[1] A.M. Mazzone, *Defect distribution in ion-implanted silicon–A Monte-Carlo simulation*, Phys. Status Solidi A 95 (1986), pp. 149–154.
[2] O.W. Holland, L. Xie, B. Nielsen, and D.S. Zhou, *Implantation of Si under extreme conditions: the effects of high temperature and dose on damage accumulation*, J. Electron. Mater. 25 (1996), pp. 99–106.
[3] G.D. Watkins, *Angular distribution of (α, n) reactions on Be and C*, J. Phys. Soc. Jpn. 18 (1963), pp. 22–28.
[4] G.D. Watkins, *Defects in irradiated silicon: EPR and electron-nuclear double resonance of interstitial boron*, Phys. Rev. B 12 (1975), pp. 5824–5839.
[5] J.A. Van Vechten, *Enthalpy of vacancy migration in Si and Ge*, Phys. Rev. B 10 (1974), pp. 1482–1506.
[6] E.J.H. Collart, K. Weemers, N.E.B. Cowern, J. Politiek, P.H.L. Bancken, J.G.M. van Berkum, and D.J. Gravesteijn, *Low energy boron implantation in silicon and room temperature diffusion*, Nucl. Instrum. Methods Phys. Res. B 139 (1998), pp. 98–107.
[7] S. Coffa and S. Libertino, *Room-temperature diffusivity of self-interstitials and vacancies in ion-implanted Si probed by* in situ *measurements*, Appl. Phys. Lett. 73 (1998), pp. 3369–3371.
[8] S. Takeda, *An atomic model of electron-irradiation-induced defects on {113} in Si*, Jpn. J. Appl. Phys. Part 2 30 (1991), pp. L639–L642.
[9] A. Agarwal, T.E. Haynes, D.J. Eaglesham, H.-J. Gossmann, D.C. Jacobson, J.M. Poate, and Y.E. Erokhin, *Interstitial defects in silicon from 1–5 keV Si^+ ion implantation*, Appl. Phys. Lett. 70 (1997), pp. 3332–3374.
[10] A. Claverie, B. Colombeau, B. de Mauduit, C. Bonafos, X. Hebras, C. Ben Assayag, and F. Cristiano, *Extended defects in shallow implants*, Appl. Phys. A: Mater. Sci. Process. 76 (2003), pp. 1025–1033.
[11] J.L. Benton, S. Libertino, P. Kringhøj, D.J. Eaglesham, J.M. Poate, and S. Coffa, *Evolution from point to extended defects in ion implanted silicon*, J. Appl. Phys. 82 (1997), pp. 120–125.
[12] D.C. Schmidt, B.G. Svensson, M. Seibt, C. Jagadish, and G. Davies, *Photoluminescence, deep level transient spectroscopy and transmission electron microscopy measurements on MeV self-ion implanted and annealed* n*-type silicon*, J. Appl. Phys. 88 (2000), pp. 2309–2317.
[13] S. Libertino, S. Coffa, and J.L. Benton, *Formation, evolution, and annihilation of interstitial clusters in ion-implanted Si*, Phys. Rev. B 63 (2001), 195206.
[14] M. Nakamura and S. Murakami, *Evolution of photoluminescent defect clusters in proton- and copper-implanted silicon crystals during annealing*, J. Appl. Phys. 94 (2003), pp. 3075–3081.
[15] P.K. Giri, *Photoluminescence signature of silicon interstitial cluster evolution from compact to extended structure in ion-implanted silicon*, Semicond. Sci. Technol. 20 (2005), pp. 638–644.
[16] D. Pierreux and A. Stesmans, *Electron spin resonance study of paramagnetic centers in neutron-irradiated heat-treated silicon*, Phys. Rev. B 71 (2005), 115204.
[17] V.C. Venezia, D.J. Eaglesham, T.E. Haynes, A. Agarwal, D.C. Jacobson, H.-J. Gossmann, and F.H. Baumann, *Depth profiling of vacancy clusters in MeV-implanted Si using Au labeling*, Appl. Phys. Lett. 73 (1998), pp. 2980–2982.

[18] R. Kalyanaraman, T.E. Haynes, V.C. Venezia, D.C. Jacobson, H.-J. Gossmann, and C.S. Rafferty, *Quantification of excess vacancy defects from high-energy ion implantation in Si by Au labeling*, Appl. Phys. Lett. 76 (2000), pp. 3379–3381.
[19] P. Mascher, S. Dannefaer, and D. Kerr, *Positron trapping rates and their temperature dependencies in electron-irradiation silicon*, Phys. Rev. B 40 (1989), pp. 11764–11771.
[20] R. Krause-Rehberg, M. Brohl, H.S. Leipner, T. Drost, A. Polity, U. Beyer, and H. Alexander, *Defects in plastically deformed semiconductors studied by positron annihilation: silicon and germanium*, Phys. Rev. B 47 (1993), pp. 13266–13276.
[21] D.S. Zhou, O.W. Holland, and J.D. Budai, *Strain relief mechanism for damage growth during high-dose, O^+ implantation of Si*, Appl. Phys. Lett. 63 (1993), p. 3580.
[22] S.L. Ellingboe and C. Ridgway, *The production and stability of implantation-induced vacancy excesses in silicon*, Nucl. Instrum. Methods Phys. Res. B 127–128 (1997), pp. 90–93.
[23] J.S. Williams, M.J. Conway, B.C. Williams, and J. Wong-Leung, *Direct observation of voids in the vacancy excess region of ion bombarded silicon*, Appl. Phys. Lett. 78 (2001), pp. 2867–2869.
[24] A. Peeva, R. Koegler, and W. Skorupa, *Visualization of vacancy type defects in the $R_P/2$ region of ion implanted and annealed silicon*, Nucl. Instrum. Methods Phys. Res. B 206 (2003), pp. 71–75.
[25] D.J. Eaglesham, P.A. Stolk, H.-J. Gossmann, and J.M. Poate, *Implantation and transient B diffusion in Si: the source of the interstitials*, Appl. Phys. Lett. 65 (1994), pp. 2305–2307.
[26] L.H. Zhang, K.S. Jones, P.H. Chi, and D.S. Simons, *Transient enhanced diffusion without {311} defects in low energy B^+-implanted silicon*, Appl. Phys. Lett. 67 (1995), pp. 2025–2027.
[27] R.A. Brown, D. Maroudas, and T. Sinno, *Modelling point defect dynamics in the crystal growth of silicon*, J. Cryst. Growth 137 (1994), pp. 12–25.
[28] V.C. Venezia, T.E. Haynes, A. Agarwal, L. Pelaz, H.-J. Gossmann, D.C. Jacobson, and D.J. Eaglesham, *Mechanism for the reduction of interstitial supersaturation in MeV-implanted silicon*, Appl. Phys. Lett. 74 (1999), pp. 1299–1301.
[29] M.T. Zawadzki, W. Luo, and P. Clancy, *Tight-binding molecular dynamics study of vacancy-interstitial annihilation in silicon*, Phys. Rev. B 63 (2001), 205205.
[30] G.S. Hwang and W.A. Goddard, III, *Diffusion and dissociation of neutral divacancies in crystalline silicon*, Phys. Rev. B 65 (2002), 233205.
[31] G.S. Hwang and W.A. Goddard, *Diffusion of the diboron pair in silicon*, Phy. Rev. Lett. 89 (2002), 055901.
[32] G.S. Hwang and W.A. Goddard, *Catalytic role of boron atoms in self-interstitial clustering in Si*, Appl. Phys. Lett. 83 (2003), pp. 1047–1049.
[33] G.S. Hwang and W.A. Goddard, *Shouldering in B diffusion profiles in Si: role of di-boron diffusion*, Appl. Phys. Lett. 83 (2003), pp. 3501–3503.
[34] C.L. Kuo, W. Luo, and P. Clancy, *A tight-binding molecular dynamics study of the dissociation of boron clusters in c-Si*, Mol. Simul. 29 (2003), pp. 577–588.
[35] S. Solmi, M. Ferri, M. Bersani, D. Giubertoni, and V. Soncini, *Transient enhanced diffusion of arsenic in silicon*, J. Appl. Phys. 94 (2003), pp. 4950–4955.
[36] M.Y.L. Jung, R. Gunawan, R.D. Braatz, and E.G. Seebauer, *A simplified picture for transient enhanced diffusion of boron in silicon*, J. Electrochem. Soc. 151 (2004), pp. G1–G7.
[37] M.Y.L. Jung, C.T.M. Kwok, R.D. Braatz, and E.G. Seebauer, *Interstitial charge states in boron-implanted silicon*, J. Appl. Phys. 97 (2005), 063520.
[38] T.A. Frewen, S.S. Kapur, W. Haeckl, W. von Ammon, and T. Sinno, *A microscopically accurate continuum model for void formation during semiconductor silicon processing*, J. Cryst. Growth 279 (2005), pp. 258–271.
[39] S.A. Harrison, T.F. Edgar, and G.S. Hwang, *Structure, stability, and diffusion of arsenic-silicon interstitial pairs*, Appl. Phys. Lett. 87 (2005), 231905.
[40] S.A. Harrison, T.F. Edgar, and G.S. Hwang, *Structure and dynamics of the diarsenic complex in crystalline silicon*, Phys. Rev. B 72 (2005), 195414.
[41] S.A. Harrison, T.F. Edgar, and G.S. Hwang, *Interstitial-mediated mechanisms of As and P diffusion in Si: gradient-corrected density-functional calculations*, Phys. Rev. B 74 (2006), 195202.
[42] S.A. Harrison, T.F. Edgar, and G.S. Hwang, *Interstitial-mediated arsenic clustering in ultrashallow junction formation*, Electrochem. Solid-State Lett. 9 (2006), pp. G354–G357.
[43] D.A. Abdulmalik and P.G. Coleman, *Activation energies for the formation and evaporation of vacancy clusters in silicon*, Phys. Rev. Lett. 100 (2008), 095503.
[44] D.J. Chadi and K.J. Chang, *Magic numbers for vacancy aggregation in crystalline Si*, Phys. Rev. B 38 (1988), pp. 1523–1525.
[45] J. Zhu, T.D. dela Rubia, L.H. Yang, C. Mailhiot, and G.H. Gilmer, Ab initio *pseudopotential calculations of B diffusion and pairing in Si*, Phys. Rev. B 54 (1996), pp. 4741–4747.
[46] P.B. Rasband, P. Clancy, and M.O. Thompson, *Equilibrium concentration of defects in pure and B-doped silicon*, J. Appl. Phys. 79 (1996), pp. 8998–9011.
[47] N. Arai, S. Takeda, and M. Kohyama, *Self-interstitial clustering in crystalline silicon*, Phys. Rev. Lett. 78 (1997), pp. 4265–4268.
[48] J.L. Hastings, S.K. Estreicher, and P.A. Fedders, *Vacancy aggregates in silicon*, Phys. Rev. B 56 (1997), pp. 10215–10220.
[49] A. Bongiorno, L. Colombo, and T. Diaz de la Rubia, *Structural and binding properties of vacancy clusters in silicon*, Europhys. Lett. 43 (1998), pp. 695–700.
[50] J. Kim, F. Kirchhoff, W.G. Aulbur, J.W. Wilkins, F.S. Khan, and C. Kresse, *Thermally activated reorientation of Di-interstitial defects in silicon*, Phys. Rev. Lett. 83 (1999), pp. 1990–1993.
[51] B.J. Coomer, J.P. Goss, R. Jones, S. Öberg, and P.R. Briddon, *Interstitial aggregates and a new model for the I_1/W optical centre in silicon*, Physica B 273–274 (1999), pp. 505–508.
[52] J. Kim, F. Kirchhoff, J.W. Wilkins, and F.S. Khan, *Stability of Si-interstitial defects: from point to extended defects*, Phys. Rev. Lett. 84 (2000), pp. 503–506.
[53] S.K. Estreicher, M. Gharaibeh, P.A. Fedders, and P. Ordejón, *Unexpected dynamics for self-interstitial clusters in silicon*, Phys. Rev. Lett. 86 (2001), pp. 1247–1250.
[54] M.P. Chichkine and M.M. de Souza, *Dynamics of self-interstitial cluster formation in silicon*, Phys. Rev. B 66 (2002), 045205.
[55] D.A. Richie, J. Kim, S.A. Barr, K.R.A. Hazzard, R. Hennig, and J.W. Wilkins, *Complexity of small silicon self-interstitial defects*, Phys. Rev. Lett. 92 (2004), 045501.
[56] G.M. Lopez and V. Fiorentini, *Structure, energetic, and extrinsic levels of small self-interstitial clusters in silicon*, Phys. Rev. B 69 (2004), 155206.
[57] L.A. Marqués, L. Pelaz, P. Castrillo, and J. Barbolla, *Molecular dynamics study of the configurational and energetic properties of the silicon self-interstitial*, Phys. Rev. B 71 (2005), 085204.
[58] M. Cogoni, B.P. Uberuaga, A.F. Voter, and L. Colombo, *Diffusion of small self-interstitial clusters in silicon: temperature-accelerated tight-binding molecular dynamics simulations*, Phys. Rev. B 71 (2005), 121203.
[59] M. Posselt, F. Gao, and D. Zwicker, *Atomistic study of the migration of di- and tri-interstitials in silicon*, Phys. Rev. B 71 (2005), 245202.
[60] A. Carvalho, R. Jones, J. Coutinho, and P.R. Briddon, *Density-functional study of small interstitial clusters in Si: comparison with experiments*, Phys. Rev. B 72 (2005), 155208.
[61] S.A. Centoni, B. Sadigh, G.H. Gilmer, T.J. Lenosky, T.D. de la Rubia, and C.B. Musgrave, *First-principles calculation of intrinsic defect formation volumes in silicon*, Phys. Rev. B 72 (2005), 195206.
[62] Y.A. Du, R.G. Hennig, T.J. Lenosky, and J.W. Wilkins, *From compact point defects to extended structures in silicon*, Eur. Phys. J. B 57 (2007), pp. 229–234.
[63] M. Saito and A. Oshiyama, *Lifetimes of positrons trapped at Si vacancies*, Phys. Rev. B 53 (1996), pp. 7810–7814.
[64] A. La Magna, S. Coffa, and L. Colombo, *Role of extended vacancy-vacancy interaction on the ripening of voids in silicon*, Phys. Rev. Lett. 82 (1999), pp. 1720–1723.
[65] G. Amarendra, R. Rajaraman, G.V. Rao, K.G.M. Nair, B. Viswanathan, R. Suzuki, T. Ohdaira, and T. Mikado, *Identification of open-volume defects in disordered and amorphized Si: a depth-resolved positron annihilation study*, Phys. Rev. B 63 (2001), 224112.

[66] S. Chakravarthi and S.T. Dunham, *Modeling of vacancy cluster formation in ion implanted silicon*, J. Appl. Phys. 89 (2001), pp. 4758–4765.
[67] T.E.M. Staab, A. Sieck, M. Haugk, M.J. Puska, Th. Frauenheim, and H.S. Leipner, *Stability of large vacancy clusters in silicon*, Phys. Rev. B 65 (2002), 115210.
[68] D.V. Makhov and L.J. Lewis, *Stable fourfold configurations for small vacancy clusters in silicon from* ab initio *calculations*, Phys. Rev. Lett. 92 (2004), 255504.
[69] B.P. Haley, K.M. Beardmore, and N. Grønbech-Jensen, *Vacancy clustering and diffusion in silicon: kinetic lattice Monte Carlo simulations*, Phys. Rev. B 74 (2006), 045217.
[70] S. Dannefaer, V. Avalos, and O. Andersen, *Grown-in vacancy-type defects in poly- and single crystalline silicon investigated by positron annihilation*, Eur. Phys. J. Appl. Phys. 37 (2007), pp. 213–218.
[71] S. Lee and G.S. Hwang, *Structure and stability of small compact-interstitial clusters in crystalline silicon*, Phys. Rev. B 77 (2008), 085210.
[72] S. Lee and G.S. Hwang, *Growth and shape transition of small silicon self-interstitial clusters*, Phys. Rev. B 78 (2008), 045204.
[73] S. Lee and G.S. Hwang, *Theoretical determination of stable coordinated vacancy clusters in silicon*, Phys. Rev. B 78 (2008), 125310.
[74] F. Wooten, K. Winer, and D. Weaire, *Computer generation of structural models of amorphous Si and Ge*, Phys. Rev. Lett. 54 (1985), pp. 1392–1395.
[75] Y.H. Tu, J. Tersoff, G. Grinstein, and D. Vanderbilt, *Properties of a continuous-random-network model for amorphous systems*, Phys. Rev. Lett. 81 (1998), pp. 4899–4902.
[76] T.J. Lenosky, J.D. Kress, I. Kwon, A.F. Voter, B. Edwards, D.F. Richards, S. Yang, and J.B. Adams, *Highly optimized tight-binding model of silicon*, Phys. Rev. B 55 (1997), pp. 1528–1544.
[77] J.P. Perdew and Y. Wang, *Accurate and simple analytic representation of the electron-gas correlation energy*, Phys. Rev. B 45 (1992), pp. 13244–13249.
[78] G. Kresse and J. Furthmuller, *VASP: the Guide*, Vienna University of Technology, Vienna, 2001.
[79] D. Vanderbilt, *Soft self-consistent pseudopotentials in a generalized eigenvalue formalism*, Phys. Rev. B 41 (1990), pp. 7892–7895.
[80] N.E. Cowern, G. Mannino, P.A. Stolk, F. Roozeboom, H.G.A. Huizing, J.G.M. van Berkum, F. Cristiano, A. Claverie, and M. Jaraíz, *Energies of self-interstitial clusters in Si*, Phys. Rev. Lett. 82 (1999), pp. 4460–4463.
[81] C.J. Ortiz, P. Pichler, T. Fühner, F. Cristiano, B. Colombeau, N.E.B. Cowern, and A. Claverie, *A physically based model for the spatial and temporal evolution of self-interstitial agglomerates in ion-implanted silicon*, J. Appl. Phys. 96 (2004), pp. 4866–4877.
[82] M. Kohyama and S. Takeda, *Atomic structure and energy of the {113} planar interstitial defects in Si*, Phys. Rev. B 46 (1992), pp. 12305–12315.
[83] J. Kim, J.W. Wilkins, F.S. Khan, and A. Canning, *Extended Si {311} defects*, Phys. Rev. B 55 (1997), pp. 16186–16197.
[84] P. Alippi and L. Colombo, *Lattice-strain field induced by {311} self-interstitial defects in silicon*, Phys. Rev. B 62 (2000), pp. 1815–1820.
[85] J.P. Goss, T.A.G. Eberlein, R. Jones, N. Pinho, A.T. Blumenau, T. Frauenheim, P.R. Briddon, and S. Öberg, *Planar interstitial aggregates in Si*, J. Phys.: Condens. Matter 14 (2002), pp. 12843–12853.
[86] P.A. Stolk, H.-J. Gossmann, D.J. Eaglesham, D.C. Jacobson, C.S. Rafferty, G.H. Gilmer, M. Jaraíz, J.M. Poate, H.S. Luftman, and T.E. Haynes, *Physical mechanisms of transient enhanced dopant diffusion in ion-implanted silicon*, J. Appl. Phys. 81 (1997), pp. 6031–6050.
[87] P. Alippi and L. Colombo, *Lattice-strain field induced by {311} self-interstitial defects in silicon*, Phys. Rev. B 62 (2000), pp. 1815–1820.